Estimating bulk rheological properties of flowing snow avalanches from field data

C. Ancey[1] and M. Meunier

Research Unit Torrential Erosion, Snow and Avalanches, Cemagref, Domaine Universitaire, Saint-Martin-d'Hères, France

Received 21 March 2003; revised 12 November 2003; accepted 2 December 2003; published 24 January 2004.

[1] Knowing the path profile and the avalanche velocity variations with downstream distance makes it possible to deduce the bulk frictional force experienced by an avalanche during its course. This derivation was applied to 15 documented events reported in the literature. Three types of rheological behavior were identified: (1) the inertial regime, where the frictional force drops to zero; (2) the Coulombic frictional force, where the force is fairly independent of the avalanche velocity; and (3) the velocity-dependent regime, where the force exhibits a complicated (nonlinear and hysteretic) dependence on velocity. During its course an avalanche can experience one or several regimes. Interestingly, the Coulomb model can provide predictions of the velocity and run-out distance in good agreement with field data for most events, even though for some path sections the bulk frictional force departs from the Coulomb model. This result is of primary importance in zoning applications since it makes it possible to deduce avalanche velocities from a knowledge of the run-out distance. Its physical meaning is, however, not clearly demonstrated in this paper due to the lack of suitable data. *INDEX TERMS:* 1863 Hydrology: Snow and ice (1827); 8160 Tectonophysics: Rheology—general; *KEYWORDS:* snow avalanche, rheological properties, Coulomb model

Citation: Ancey, C., and M. Meunier (2004), Estimating bulk rheological properties of flowing snow avalanches from field data, *J. Geophys. Res.*, *109*, F01004, doi:10.1029/2003JF000036.

1. Introduction

[2] A number of natural gravity-driven flows, such as debris and snow avalanches, take the appearance of a fluid stream flow. When interested in determining the properties of these mass movements, it can be fruitful to develop the fluid analogy by using a fluid mechanics treatment and considering such flows as one-phase flows at a macroscopic scale, although at a microscopic scale the materials can involve two or three phases. Such a framework has been developed in the field of snow avalanches [*Brugnot and Pochat*, 1981; *Eglit*, 1983], lava flows [*Balmforth et al.*, 2000], mudflows [*Coussot*, 1997], debris flows [*Iverson and Denlinger*, 2001], debris avalanches and rock falls [*Savage*, 1989; *Hutter et al.*, 1995; *Tai et al.*, 2001], and turbidity currents [*Parker et al.*, 1986].

[3] Within this framework a key point is to determine the bulk rheological properties of the materials. For fine materials involved in mudflows and lava, using laboratory rheometers makes it possible to infer the rheological properties from rheometrical data [*Spera et al.*, 1988; *Major and Pierson*, 1992; *Coussot*, 1997]. For coarse-grained materials involved in debris flows, this procedure is more complicated to use and often leads to results that are difficult to interpret from a rheological viewpoint [*Contreras and Davies*, 2000]. An alternative approach is to develop theoretical constitutive equations and test them against large-scale channel experiments [*Denlinger and Iverson*, 2001]. This, however, requires that the flow conditions and the materials used in the reduced-scale experiment fulfill similarity conditions relative to full-scale events [*Iverson*, 1997; *Iverson and Denlinger*, 2001].

[4] Snow avalanches occupy a particular position in that, in contrast to lava and debris flows, there are no sound field or laboratory data available on the basic rheological processes involved in avalanche release and flow. Therefore all the avalanche dynamics models proposed so far rely on analogy with other physical phenomena: Typical examples include analogies with granular flows [*Savage and Hutter*, 1989; *Savage*, 1989; *Hutter and Greve*, 1993; *Tai et al.*, 2001], Newtonian fluids [*Hunt*, 1994], power law fluids [*Norem et al.*, 1986], and viscoplastic flows [*Dent and Lang*, 1982; *Ancey*, 2001b]. From a purely rheological point of view, these models rely on a purely speculative foundation. Indeed, most of the time, the rheological parameters used in these models have been estimated by matching the model predictions (such as the leading edge velocity and the run-out distance) with field data [*Schaerer*, 1974; *Buser and Frutiger*, 1980; *Dent and Lang*, 1980]. However, this obviously does not provide evidence that the constitutive equation is appropriate. A number of experiments on snow have also been done in the laboratory. Authors such as *Dent and Lang* [1982] and *Maeno* [1993] have measured the

[1]Now at Environmental Hydraulics Laboratory, Swiss Federal Institute of Technology, Lausanne, Switzerland.

Copyright 2004 by the American Geophysical Union.
0148-0227/04/2003JF000036$09.00

velocity profile within snow flows and generally deduced that snow generates a non-Newtonian viscoplastic flow, whose properties depend a great deal on density. Transposing these laboratory results to real avalanches is not clearly reliable due to size-scale effects and similarity conditions. Furthermore, given the severe difficulties inherent to snow rheometry (sample fracture during shearing tests, variation in the snow microstructure resulting from thermodynamic transformations of crystals, etc.), properly identifying the constitutive equation of snow with modern rheometers is out of reach for the moment.

[5] The objective of this paper is to present a novel method for deducing the bulk rheological properties of gravity-driven flows from field data. Here, in the applications, emphasis is given to snow avalanches, but the method can also be applied to a wide range of mass movements. In accordance with the terminology adopted by practitioners [*de Quervain*, 1981; *McClung and Schaerer*, 1993], we use the term "flowing avalanches" to refer to snow avalanches with a high-density core at the bottom. On average, the density is fairly high, ranging from 150 kg m^{-3} to 500 kg m^{-3}. The flow depth does not generally exceed a few meters (typically 1–2 m). Snow involved in the avalanche can be of varying consistency: granular (snowball), loose (slush snow), pasty, etc. Flowing avalanches differ from airborne (or powder snow) avalanches in several respects: Taking the form of a dilute turbulent cloud, airborne avalanches can reach very high velocities (as high as 100 m s^{-1}); the flow depth is large (typically in the range 20–100 m) and grows continuously as a result of air entrainment when the avalanche descends; and the average bulk density is fairly low (in the range 1–25 kg m^{-3}) [*McClung and Schaerer*, 1993; *Ancey*, 2003]. The method presented here does not apply to this flow family, whose dynamics are controlled by buoyancy effects rather than by rheological properties.

[6] This paper will begin by presenting the method used for deriving the bulk frictional force. Essentially, we will show that knowing the path profile and the front avalanche velocity can make it possible to calculate the frictional force experienced by the avalanche. We will then apply the method to 15 documented events reported in the technical literature and demonstrate that at least three regimes can be identified by examining the variation in the bulk frictional force with avalanche velocity: In an inertial regime, the frictional force is very low relative to the driving force; in a Coulomb frictional regime, the frictional force is independent of the velocity; while in a velocity-dependent regime, the frictional force reveals a complex pattern, including a hysteretic behavior. Lastly, we will discuss the results obtained with this method. A key question must be raised: Do we really understand the physics when using the proposed simplified treatment, or, in other words, does the flow regime identified as a Coulomb frictional regime reflect Coulomb rheological behavior at the microscopic scale?

2. Methodology

2.1. Determining Bulk Rheological Properties From Flow Properties

[7] In most fluid mechanics problems the constitutive equation and the boundary conditions are known in advance, and the equations of motion are solved to determine flow features such as the discharge equation (relationship between flow rate and flow depth). The inverse problem starts from the knowledge of certain flow characteristics to deduce the constitutive behavior of the material involved.

[8] In the simplest fluid mechanics treatment of natural flows the bulk material is considered as a whole at the macroscopic scale; the local momentum balance equation is written as

$$\rho \frac{d\mathbf{u}}{dt} = \rho \mathbf{g} - \nabla p + \nabla \cdot \Sigma, \tag{1}$$

where ρ denotes bulk density, $\mathbf{u}$ denotes velocity, $\mathbf{g}$ denotes gravity acceleration, p denotes pressure, Σ denotes bulk extra stress tensor, and $d \cdot /dt$ denotes the material derivative. Let us now consider a steady uniform isochoric flow of a bulk material down an infinite plane inclined at an angle θ. These simple shear flow assumptions make it possible to substantially simplify the equations of motion. It can be shown that under these conditions, at a depth $h - y$ from the free surface, where h is the total flow depth, the shear stress is $\tau = \rho g \sin\theta\,(h - y)$ (see *Ancey et al.* [1996a] and *Ancey* [2001a] for the details of the derivation). This shear stress is related to the shear rate $\dot{\gamma} = du/dy$ via the constitutive equation. In the case of a simple fluid the constitutive equation takes the form of a one-to-one relationship between $\dot{\gamma}$ and τ that here is denoted G: $\dot{\gamma} = G(\tau)$. If this function is known, we can compute the depth-averaged velocity $\bar{u} : h\bar{u} = \int_0^h u(y)dy = \int_0^h dy \int_0^y \dot{\gamma}(\eta)d\eta$. conversely, knowing the mean velocity $\bar{u}(h)$ makes it possible to infer the flow curve. Indeed, using an integration by parts, then differentiating with respect to h, we obtain

$$\dot{\gamma} = G(\tau_b) = \frac{1}{h}\left(\frac{\partial h\bar{u}}{\partial h}\right)_\theta, \tag{2}$$

where τ_b is the bottom shear stress ($\tau_b = \rho g h \sin\theta$). This equation shows that the flow curve $\dot{\gamma} = G(\tau)$ can be directly deduced from the measurement of flow depth h and mean flow velocity $\bar{u}$. In theory, this provides us with the means of deriving the rheological behavior from field measurements $\bar{u}(h)$. In practice, however, this expression is of limited interest given how difficult it is to obtain field measurements of both the flow depth and mean velocity. Moreover, natural flow conditions are far from the purely viscometric flow conditions that underlie the computations above.

[9] However, the idea deserves further development by simplifying the equations of motion. Here the simplest case where the fluid can be considered a slender sliding body, of volume V and possibly of varying mass m, is examined. The variations in body shape are ignored in a first approximation (A1). The body moves along a curvilinear two-dimensional profile, whose equation in a Cartesian frame takes the form $y = f(x)$, where y is the elevation and x is an arbitrary distance measured along a horizontal axis. In doing so, it is implicitly assumed that there is no significant lateral spreading of the mass (A2). In the following we assume that the path profile is a smooth and gently varying curve (A3). Basically, this means that the curvature radius $R = (1 + f'^2(x))^{3/2}/f''(x)$ is at least as large as the typical length L scale of the flow or larger: $R \sim L$ or $R > L$. The position of the

center of mass is given by its curvilinear abscissa $\xi = \int_0^x \sqrt{1+f'^2(x)}dx$ taken from an arbitrary point of origin; we have $x = \xi \cos \bar{\theta}$, with $\bar{\theta}$ the mean path inclination computed over the interval $[0, x]$. The ordinate of the center of mass (relative to the curve f) is denoted η; assumption A1 implies that η is fairly constant and the velocity in the η direction is close to zero. The velocity in the ξ direction is $u = (1 - \eta/R)d\xi/dt$. The bulk equation of motion can be deduced by integrating the local motion equation (1) over the volume V. The downward and normal components of the momentum equation can be expressed as

$$\left(1-\frac{\eta}{R}\right)\frac{d^2\xi}{dt^2}+\frac{\eta}{R^2}\frac{dR}{d\xi}\left(\frac{d\xi}{dt}\right)^2 = g\sin\theta(\xi) - S\frac{\tau_b}{m} - \frac{1}{m}\left(1-\frac{\eta}{R}\right)\frac{d\xi}{dt}\frac{dm}{dt} \quad (3)$$

$$-\frac{1}{R-\eta}\left(\frac{d\xi}{dt}\right)^2 = -g\cos\theta(\xi) + S\frac{\sigma_b}{m}, \quad (4)$$

where S is the surface of the body in contact with the sliding plane and (τ_b, σ_b) are the average shear and normal stresses at the bottom. In the left-hand side of equation (3) the first term represents the downward component of the acceleration, while the second term reflects radial effects due to the curvature of the path profile. In the right-hand side of equation (3) the first contribution is the driving action of gravity, the second term stands for the frictional force exerted by the bottom (ground or snow cover) on the avalanche, while the last term reflects the momentum variations induced by the variation in mass with time.

[10] These equations can be simplified a great deal by assuming that the mass variations can be neglected (A4) and that the curvature radius is very large relative to the depth η: $R \gg \eta$ (A5). The latter assumption means that everything happens locally, as if the path were an infinite plane inclined at an angle $\tan \theta(x) = f'(x)$ with respect to the horizontal. Under these assumptions we have $u = d\xi/dt$, and equations (3) and (4) can be cast into the simplified form

$$\frac{S}{m}\tau_b = g\sin\theta(\xi) - u\frac{du}{d\xi} \quad (5)$$

$$\frac{S}{m}\sigma_b = g\cos\theta(\xi), \quad (6)$$

where we used $du/dt = udu/d\xi$. Given assumptions A1, A2, and A4, the ratio S/m is constant in the equations of motion. The interpretation of equation (5) is clear: If one has a record yielding the body velocity as a function of the position along the path, then it is possible to directly deduce the bottom shear stress and its relationship with the velocity u to a multiplicative factor S/m. To first order, the average bottom normal stress only depends on the local slope: $mg \cos \theta(\xi)/S$. Equation (5) should provide the main trends of the rheological behavior. Plotting the resulting force per unit mass in a phase space (u, σ_b, τ_b) can give an idea of the dependence of the frictional force on the mean velocity and normal component.

[11] Owing to the number of assumptions and approximations (A1–A5) made to arrive at this expression, it may be uncertain whether the bulk rheological behavior is properly reflected by a simplified expression in the form of equation (5). Indeed, a number of additional contributions may be hidden in the bulk frictional force determined by equation (5). For instance, if assumption (A4) does not hold, i.e., there is a mass variation during the course of the avalanche, the bottom shear stress must be corrected by the quantity $-u^2(dm/d\xi)/S$. Similarly, a sudden variation in the path profile induces a radial acceleration in the form $u^2/R(\xi)$. Moreover, the physical properties of the snow volume involved in the avalanche may vary when the avalanche descends: snow compaction, air entrainment and formation of a cloud of snow particles above the core, increase in the water content leading to the development of snowballs, etc. Singularities along the path, such as a sudden widening or turn, may influence the body motion and add additional terms to F. However, it is expected that, on the whole, equation (5) can capture the essential traits of the bulk frictional force experienced by the avalanche.

2.2. Practical Use

[12] Equation (2) provides a fairly rigorous way of inferring the bottom shear rate as a function of the shear stress by assimilating a natural flow to a viscometric flow, but its applicability is limited due to stringent assumptions of flow conditions and a dearth of field data $(\bar{u}, h)$ for natural events. For snow avalanches we found no available data in the literature. Equation (5) provides a cruder way of relating the shear stress to the flow velocity (to a multiplicative factor), but it is less data hungry than equation (2) since only the knowledge of $u(\xi)$ along the path profile is needed. In the following we will use this equation for determining the bulk rheological properties of snow avalanches.

[13] In practice, the data treatment can be broken down into two steps. The first step is to denoise the recorded data. Indeed, in equation (5) the bulk shear stress is deduced by determining the local path slope and the ξ derivative of the velocity. In absence of data smoothing the shear stress deduced from equation (5) is very noisy due to the amplification of discretization errors. To reduce the noise, the best polynomial approximations of the discretized velocity and path profiles is sought. Here $\tilde{v}(\xi)$ and $\tilde{f}(\xi)$ denote the N-order polynomial approximations of the velocity and path profiles, while v_i $(1 \le i \le q)$ and f_i $(1 \le i \le n)$ represent the recorded velocity and the discretization points of the path profile at a given set of path points ξ_i. Using orthogonality properties of Legendre polynomials, one writes the polynomials $\tilde{v}(\xi)$ and $\tilde{f}(\xi)$ as $\tilde{v}(\xi) = \Sigma_k \alpha_k P_k(r)$ and $\tilde{f}(\xi) = \Sigma_k \beta_k P_k(r)$, $0 \le k \le N$, where $P_k(\xi) = \gamma_k d^k(s^2 - 1)^k/d\xi^k$ is the normalized Legendre polynomial of order k, defined over the range $[-1, 1]$, $\gamma_k = \sqrt{2k+1}/(2^k k!\sqrt{2})$ is the normalizing constant, and r is the scaled variable defined by $r(\xi) = (2\xi - (\xi_1 + \xi_p))/(\xi_p - \xi_1)$, with index $p = n$ or $p = q$, depending on whether r is related to the variation of the path profile or the velocity. The coefficients α_k (similarly β_k) are determined using the least squares method, i.e., by minimizing the functional $J = \Sigma_i(f_i - \Sigma_k \alpha_k P_k(r_i))^2$.

[14] In the second step we studied the relationship between the shear stress deduced from equation (5) and the velocity and the slope. In fact, equation (5) displays the ratio of the frictional force to the avalanche mass $F/m = S\tau_b/m$ rather than the shear stress alone; thus in the following we

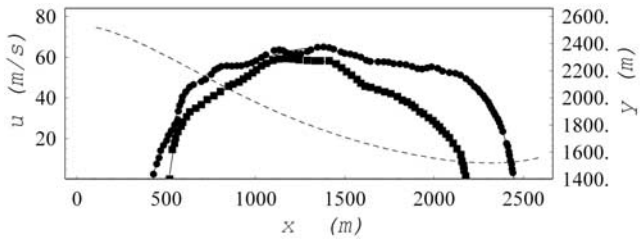

Figure 1. Path profile (dashed curve) of the Aulta site and front velocities for the avalanches of 8 February 1984 (dots) and 10 February 1984 (squares). The path profile was obtained by interpolating the discretization points with a series of Legendre polynomials (N = 17). The same was done with the velocity data (solid line, N = 10).

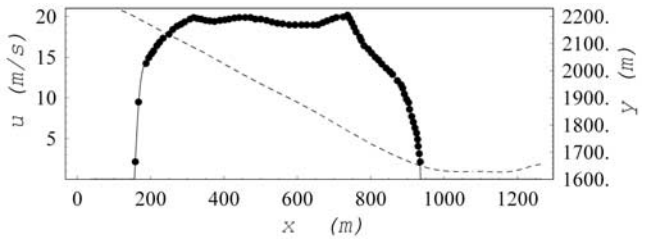

Figure 3. Path profile (dashed curve) of the Fogas site and front velocities for the avalanches of 7 March 1985. The path profile was obtained by interpolating the discretization points with a series of Legendre polynomials (N = 17). The same was done with the velocity data (solid line, N = 23).

will consider the ratio F/m instead of τ_b. It is usually easier to perform the computations in the fixed Cartesian frame (x, y) and then compute the acceleration in the curvilinear frame by using the relation between the ξ and x derivatives of the velocity: $u'(\xi) = u'(x)\cos\theta(x)$. For each event a three-dimensional parametric plot, relating F/m as a function of $u(s)$ and $\sin\theta$, can be plotted to identify the rheological behavior. The resulting curve is, however, difficult to interpret, and in practice, it is easier to examine the variation $F(u)/m$ alone.

3. Application and Results

[15] The inference method presented in section 2.2 has been applied in the context of snow avalanches. The literature was searched to find field data, including both the path profile and the velocity variation along the path. Though a large number of field surveys have been carried out in many countries over the last 30 years, we have found only a very limited number of events that satisfy our constraints: In all, only 15 events have been sufficiently documented. Raw data are presented in section 3.1 (Figures 1–7).

[16] We applied equation (5) to these field data. Figure 8 shows a snapshot of the results. The observed behavior is quite complex and is probably best explained by describing the main trends. To that end, we have considered three distinct regimes or phases depending on the frictional force variation relative to u and the driving force $mg\sin\theta$: (1) the inertial regime, for which gravitational force outweighs frictional force (section 3.2); (2) the Coulombic frictional regime, for which frictional force is fairly constant and independent of velocity (section 3.3); and (3) the velocity-dependent regimes, for which frictional force reveals a complicated dependence on velocity that can be approximated by a power law relation (section 3.4). As shown in sections 3.2–3.4, the motion of an avalanche can be described as the occurrence of a single regime or the succession of two or three regimes. For instance, the inertial regime was observed only for the release phase; at later times the avalanches reached a Coulombic frictional and/or velocity-dependent regime(s).

3.1. Raw Data

[17] Table 1 summarizes the main features of these events. *Gubler et al.* [1986] recorded the velocity variations for six events in three distinctive paths in Switzerland: Aulta (see Figure 1), Madergrond (see Figure 2), and Fogas (see Figure 3). *Kotlyakov et al.* [1977] measured velocity variations for three events in a single path in the Khibins in Russia (see Figure 4). *Sovilla et al.* [2001] measured velocity and mass balance for four events at the Arabba site in Italy (see Figure 5). *LaChapelle and Lang* [1980] provided a velocity record for an avalanche in the Shlushman path in Colorado (see Figure 6). Our laboratory recorded velocity several times at the Lautaret site (France), but only one of these records provides the variation in front velocity with distance (see Figure 7) [*Marco*, 1986]. In each of Figures 1–7 we have reported the interpolated path

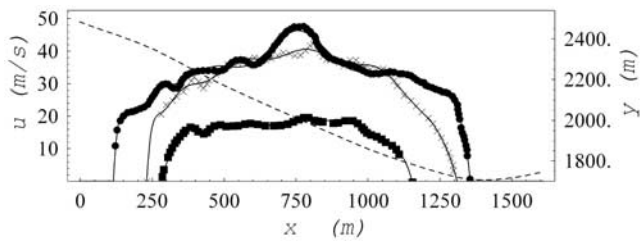

Figure 2. Path profile (dashed curve) of the Madergrond site and front velocities for the avalanches of 17 January 1985: avalanche a (dots), b (squares), and c (crosses). The path profile was obtained by interpolating the discretization points with a series of Legendre polynomials (N = 15). The same was done with the velocity data (solid line, N = 15).

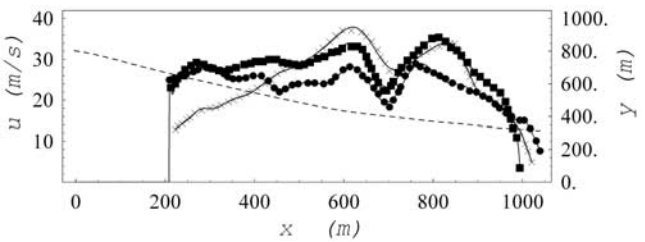

Figure 4. Path profile (dashed curve) of the Khibins site and front velocities: avalanche a (dots), b (squares), and c (crosses). The path profile was obtained by interpolating the discretization points with a series of Legendre polynomials (N = 17). The same was done with the velocity data (solid line, N = 23).

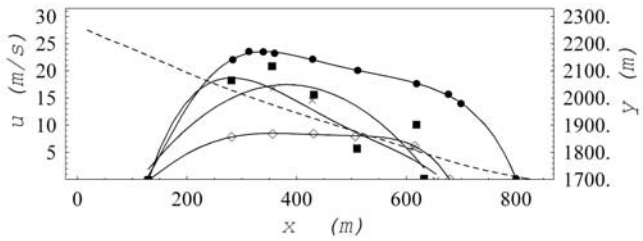

Figure 5. Path profile (dashed curve) of the Arabba site and front velocities for the avalanches of 21 December 1997 (dots), 14 April 1998 (squares), 5 December 1997 (crosses), and 14 December 1997 (diamonds). The path profile was obtained by interpolating the discretization points with a series of Legendre polynomials (N = 10). The same was done with the velocity data (solid line, N = 7).

profile (dashed line) together with measured (symbols) and interpolated (solid line) velocities.

[18] Note that the quality of data varies from one event to another depending on how data were acquired. Avalanche velocity is most often measured at the front using image processing techniques (video tapes) or stereo-photogrammetry. In some cases (for the events recorded in Switzerland) the front velocity was determined accurately using a Doppler radar. For the Swiss events the data number is large, which allows us to interpolate the velocity data with a high degree of confidence from release to run-out. For the Lautaret avalanche the velocity was measured for only four points in close vicinity; moreover, the starting and stopping points are known. In this case, it was difficult to suitably interpolate the data (see Figure 7) since we have only six data irregularly distributed along the path profile. The same comment must also be mode for the Arabba avalanche of 14 April 1998 (see Figure 5).

3.2. Avalanches in an Inertial Regime

[19] For a number of events (see Figures 1, 2, and 4) the avalanches reached high velocities (higher than 30 m s^{-1}), which indicates that the frictional forces experienced by these avalanches were low (see Figure 8). Within our simplified fluid mechanics framework the velocity cannot reach any velocity whatsoever: There is a maximum velocity, which can be computed using the free-fall approximation. Indeed, if an avalanche were in a purely inertial regime, its frictional force would be zero, and the avalanche motion would be similar to the motion of a body in free fall. In this case,

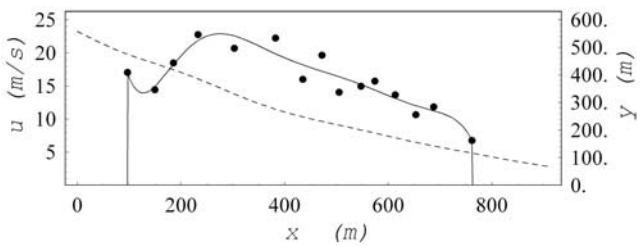

Figure 6. Path profile (dashed curve) of the Shlushman site and front velocities. The path profile was obtained by interpolating the discretization points with a series of Legendre polynomials (N = 17). The same was done with the velocity data (solid line, N = 23).

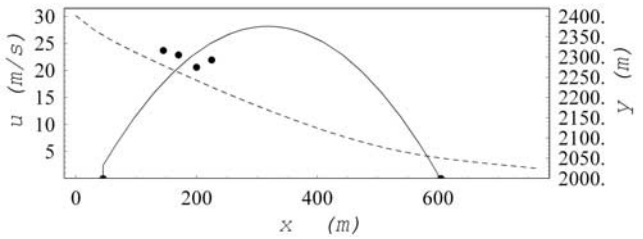

Figure 7. Path profile (dashed curve) of the Lautaret site and front velocities. The path profile was obtained by interpolating the discretization points with a series of Legendre polynomials (N = 10). The same was done with the velocity data (solid line, N = 2).

integrating the momentum equation (5) with $\tau_b = 0$, the initial condition $u = 0$ at $\xi = \xi_0$, leads to $u^2(\xi) = \int_{\xi_0}^{\xi} 2g \sin\theta(\xi')d\xi'$. There is no analytical solution to this integral, but in the case where the slope θ is not too far from a constant value $\hat{\theta}$ the following approximation holds to first order: $u(x) \approx \sqrt{2g(x - x_0)\tan\hat{\theta}}$, where x_0 is the abscissa in the Cartesian frame associated with the curvilinear abscissa ξ_0. Let us now use an example to examine how the maximum velocities reached by high-speed avalanches deviate from the maximum velocities of a purely inertial body.

[20] Figure 9 shows the force variation for the avalanche that occurred on 8 February 1984 at the Aulta site; on the same plot we have drawn the downward component of the driving force per unit mass $g \sin\theta$. In the inset of Figure 9 we have drawn the velocity variations (dashed line) if the avalanche were in a purely inertial flow (the dashed curve was obtained by solving equation (5) numerically), and we have added the measured velocities (same data as in Figure 1). The avalanches of 10 February 1984 in the Aulta path and 17 January 1985 (a and c) in the Madergrond path provide similar results (see Figures 2 and 8).

[21] As seen in the inset of Figure 9, the avalanche accelerated vigorously, and over the first 250 m it traveled, its velocity was close to the free-fall velocity (dashed curve). In fact, as shown in Figure 9, the frictional force was far from zero. It first decreased with increasing velocity and was much less than the gravity acceleration (dashed curve): On the whole, between instants A and B, the force decreased as $F/m \propto u^{-n}$, with $n = 1.05 \pm 0.1$. At instant B, at which point the recorded velocity departed from the free-fall velocity, gravity acceleration was ten times as large as the frictional force, and the avalanche reached a high velocity (35 m s^{-1}). Then, between instants B and C the frictional force increased substantially as $F/m \propto u^{4.3}$ (velocity-dependent regime), but owing to the difference between gravity acceleration and frictional force, the avalanche velocity further increased. At instant C the maximum velocity was reached (60 m s^{-1}), and the frictional and gravitational forces were approximately equal: $F/m \approx g \sin\theta$. From this instant (or equivalent from $x \approx 1100$ m) and until instant D the avalanche remained in a high-velocity regime (velocity in excess of 30 m s^{-1}). Though the slope varies significantly in the range 0.6–0.2 (see Figure 1), there was no significant variation in the frictional force. As seen in Figure 9, between instants C and D, there were large fluctuations in the frictional force around the mean value: $F/m = 4 \pm 2$ m/s^2. As a first approximation, the frictional force can be assumed to be

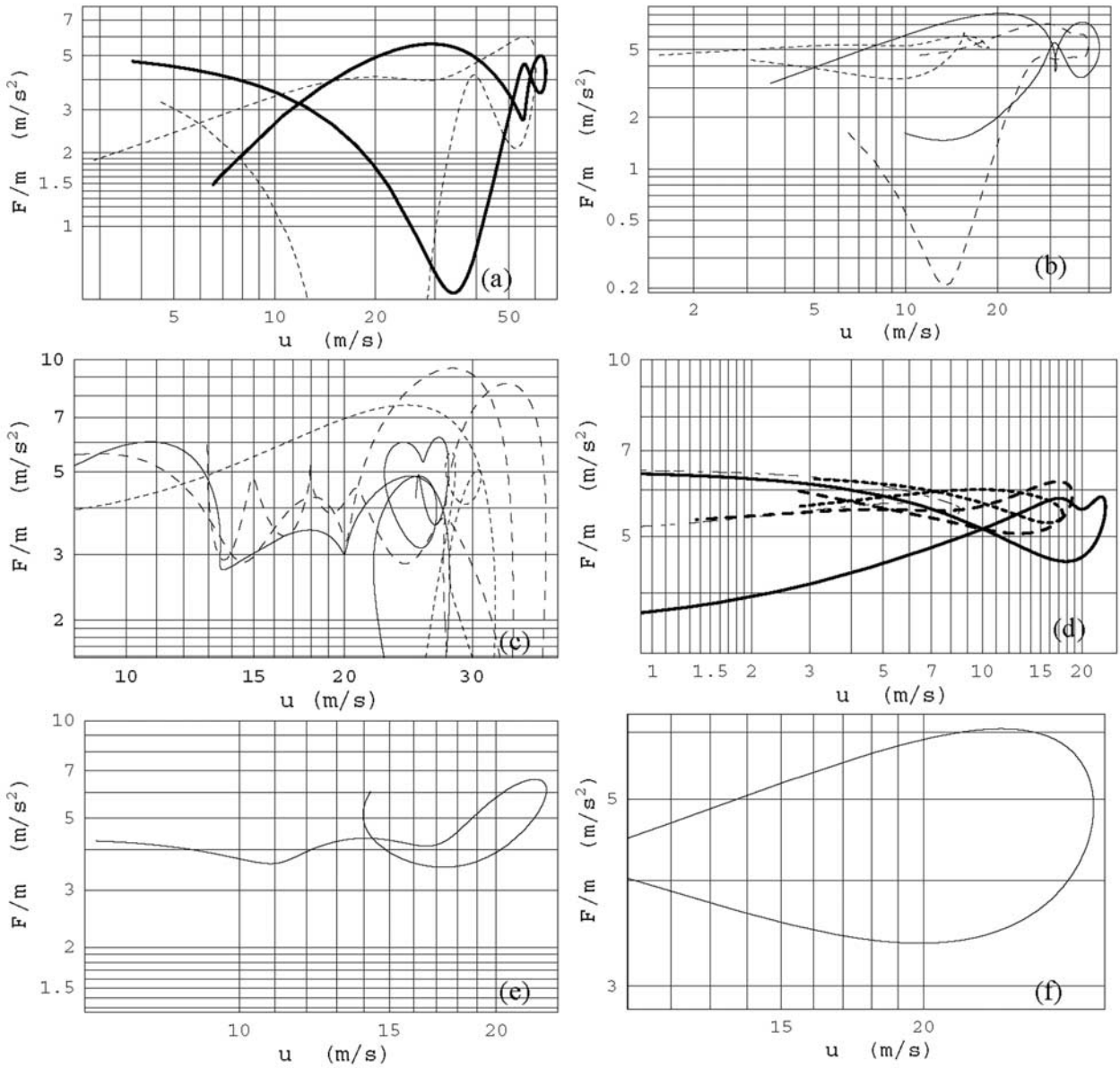

Figure 8. Variation in the frictional force per unit mass F/m with the avalanche velocity u for the documented events. (a) Aulta path: avalanche of 8 February 1984 (solid line) and avalanche of 10 February 1984 (dashed line). (b) Madergrond path: avalanches of 17 January 1986; avalanche a (solid line), avalanche b (short-dashed line), and avalanche c (long-dashed line). (c) Khibins path: avalanche a (solid line), avalanche b (short-dashed line), and avalanche c (long-dashed line). (d) Arraba path: avalanche of 21 December 1987 (solid line), avalanche of 14 April 1998 (short-dashed line), avalanche of 5 December 1997 (long-dashed line), and avalanche of 14 December 1987 (thin dashed line). (e) Slushmann path. (f) Lautaret path. For the Fogas path, see Figure 11.

constant; this means that the avalanche reached a Coulomb-like regime (see section 3.3).

[22] At $x \approx 2200$ m (point D) the avalanche suddenly decelerated. Within 250 m the avalanche velocity dropped from 50 to 0 m s^{-1}, implying that the avalanche's kinetic energy was dissipated in a short time. Interestingly enough, Figure 9 reveals no strong dependence of the frictional force on velocity, which should be the signature of a very dissipative process. Indeed, between instants D and E the frictional force varied slowly with velocity: $F/m \propto u^{0.7}$ (velocity-dependent regime).

[23] In short, the Aulta avalanche of 8 February 1984 went through four regimes: first an inertial regime, during which the avalanche accelerated as a free-fall body during the early phases, allowing it to reach very high velocities. Then, there was a phase associated with a substantial increase in the dependence of the frictional force on velocity (velocity-dependent regime). This phase marked the depar-

Table 1. Main Features of the Events Used for the Back Analysis[a]

Site Name	Date	y_0, m	L, m	θ_0, deg	θ_f, deg	Section	h_0	V, m^3	Snow Type
Aulta (a)	8 Feb. 1984	2400–2500	1550	−31	12	channeled	0.7–1	50,000	powder
Aulta (b)	10 Feb. 1984	2300–2400	1570	−37	−12	channeled	0.5–1	10,000	powder
Fogas	7 March 1985	2100–2200	780	−34	30	open	0.3	500	powder
Madergrond (a)	17 Jan. 1985	2450	1710	−25	−10	channeled	1–5	20,000	mix of new and old snow
Madergrond (b)	17 Jan. 1985	2300	1800	−33	−24	channeled	0.3–0.7	3000	mix of new and old snow
Madergrond (c)	17 Jan. 1985	2300–2400	1080	−33	−19	channeled	1–3	26,000	mix of new and old snow
Khibins (a)		700	800	−37	−14	channeled			
Khibins (b)		700	800	−37	−14	channeled			
Khibins (c)		700	800	−37	−14	channeled			
Shlushman		2660	900	−39	−19	open/channeled	1–1.5	6000	wet
Arabba (a)	21 Dec. 1997	2200	680	−40	−20	channeled	1.4	4200	powder
Arabba (b)	14 April 1998	2200	550	−40	−20	channeled	0.45	4200	wet
Arabba (c)	5 Dec. 1997	2200	550	−40	−20	channeled	0.25	500	powder
Arabba (d)	14 Dec. 1997	2200	550	−40	−20	channeled	0.45	1000	wet
Col du Lautaret	14 Feb. 1979	2350	535	−42	−13	channeled	0.2–0.5		powder snow

[a]We have reported the elevation range of the starting zone y_0, the length traveled by the avalanche L, the mean inclination of the release zone θ_0, the mean inclination of the run-out zone θ_f, the shape of the flow section, the mean thickness of the snow layer released h_0, the volume of snow involved in the avalanche, and the type of snow.

ture from the inertial regime. Afterward, the avalanche reached a fairly steady state, during which the velocity varied little: the flow regime can be described approximately as a Coulombic frictional regime. In the run-out phase the avalanche decelerated quickly; the frictional force varied almost linearly with velocity (velocity-dependent regime).

3.3. Avalanches in a Coulombic Frictional Regime

[24] For a number of events the frictional force was found to be weakly dependent on velocity or to fluctuate around a mean value during the entire course of the avalanche. Figure 10 shows a typical example provided by the avalanche in the Arraba site on 21 December 1997. The Khibins avalanches, the Lautaret avalanche, and the Arraba avalanches of 5 and 14 April 1998 were also in a Coulombic frictional regime most of the time (see Figure 8). For other events this regime was either never reached or reached only over finite periods of time (e.g., see instants C–D for the avalanche of 8 February 1984 in the Aulta path (Figure 9)).

[25] In Figure 10 we have drawn the variation in the frictional force per unit mass with velocity (solid line) and the downward component of the driving force per unit mass

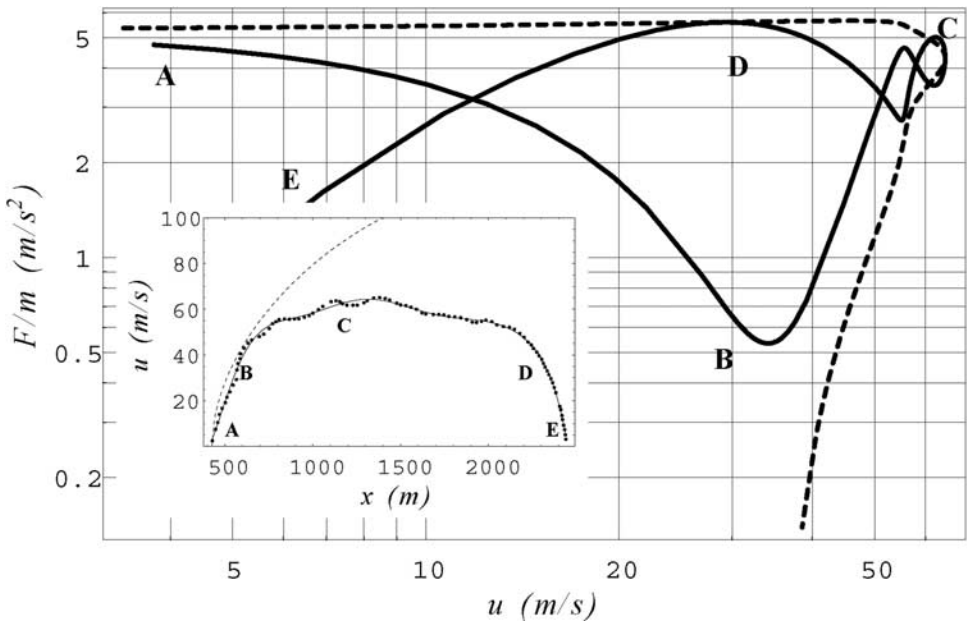

Figure 9. Variation in the frictional force per unit mass F/m with the avalanche velocity u for the avalanche of 8 December 1984 in the Aulta path (solid line); F/m was obtained by applying equation (5) to the measured velocities and path profile, both regularized using N-order Legendre polynomials ($N = 10$ for the velocities, $N = 5$ for the path profile). The dashed curve stands for the variation in the driving force per unit mass $g\sin\theta$. In the inset we have reported the variations in the measured velocities (dots) with downstream distance x. In the inset the solid line represents the Legendre polynomial approximation of velocities, while the dashed line stands for the velocity of a pure inertial flow. Letters from A to E refer to various stages of the avalanche run (see text). The starting point is $x_0 = 422$ m; the run-out point is $x_{stop} = 2440$ m.

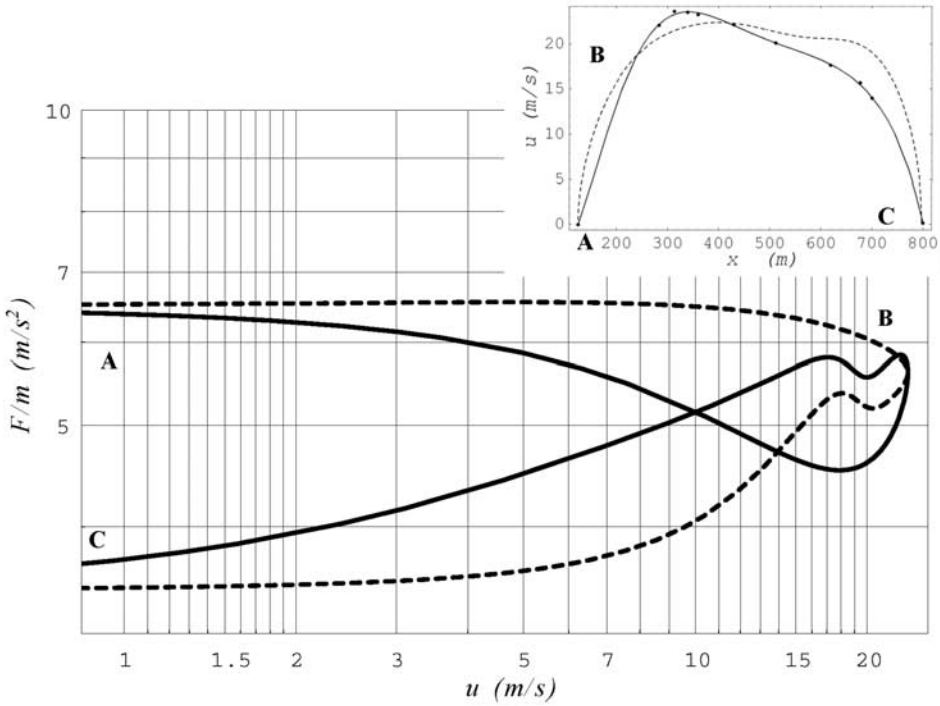

Figure 10. Variation in the frictional force per unit mass F/m with the avalanche velocity u for the avalanche of 21 December 1997 in the Arabba site (solid line); F/m was obtained by applying equation (5) to the measured velocities and path profile, both regularized using N-order Legendre polynomials ($N = 7$ for the velocities, $N = 10$ for the path profile). The dashed curve stands for the variation in the driving force per unit mass $g\sin\theta$. In the inset we have reported the variations in the measured velocities (dots) with downstream distance x. In the inset the solid line represents the Legendre polynomial approximation of velocities, while the dashed line stands for the velocity of a rigid body sliding in a pure Coulombic regime (with $\mu = 0.66$). Letters from A to C refer to various stages of the avalanche run (see text). The starting point is $x_0 = 122$ m; the run-out point is $x_{stop} = 799$ m.

$g\sin\theta$ (dashed line). In the inset we have plotted the measured velocities (dots) together with the Legendre polynomial approximation used in the computations. On the same plot we have drawn the velocity variations as if the avalanche were in a pure Coulomb regime (dashed line): Assuming that the frictional force is in the Coulombic form $F = \mu\sigma_b S = \mu mg \cos\theta$, where μ is the bulk friction coefficient, we numerically solved the equation of motion (equation (5), in which $S\tau_b/m$ is replaced with the expression of F above) using the initial condition $u(\xi_0) = 0$ in the curvilinear frame. Repeating the procedure for different values of μ (while keeping the same initial conditions) leads to a one-parameter family of curves $u(\xi|\mu)$. Since each μ curve is bell shaped, the velocity drops to zero at a given abscissa, hereinafter referred to as the run-out distance ξ_{stop}, which is a function of μ: $u(\xi_{stop}(\mu)|\mu) = 0$ (here ξ_{stop} corresponds to $x_{stop} = 800$ m in Figure 10). We selected the friction coefficient for the computed run-out distance to match the recorded value. We found that $\mu = 0.66$ for the Arabba avalanche of 21 December 1997.

[26] As shown in Figure 10, in the early phases (between points A and B) the frictional force gently decreased with increasing velocity and was slightly lower than the gravity acceleration $g \sin\theta$. Owing to the small difference between $g\sin\theta$ and F/m, the avalanche accelerated less vigorously than an avalanche in an inertial regime. At instant B the avalanche reached its maximum velocity (24 m s^{-1}). At this point the frictional force started exceeding the gravitational force, and the avalanche decelerated monotonically. Obviously, the frictional force did depend on the avalanche velocity, as shown in Figure 4, but this dependence remained slight since between B and C we have $F/m \propto u^{0.1 \pm 0.05}$. Thus as a first approximation, the frictional force can be considered constant between instants A and C: $F/m = 5 \pm 1.3$ m s^{-2}. As shown in the inset of Figure 10, the computed velocities obtained by assuming a pure Coulombic regime (dashed curve) compare well with the data: Like the recorded values, the computed velocities exhibit an asymmetric U-shaped form, while the relative deviation between the two curves is <20%.

3.4. Avalanches in a Velocity-Dependent Regime

[27] Frictional force depending on the velocity can be interpreted as the signature of a fluid behavior of avalanches. For each documented event we looked for a scaling of frictional force in the form $F/m \propto u^n$. In section 3.2 we saw that the Aulta avalanche of 8 February 1984 revealed a velocity-dependent regime in the accelerating phase $F/m \propto u^{4.3}$ and in the decelerating phase $F/m \propto u^{0.7}$. Note the substantial difference in scaling. For other avalanches we also found that frictional force could depend on velocity during the decelerating and/or the accelerating phase(s), but

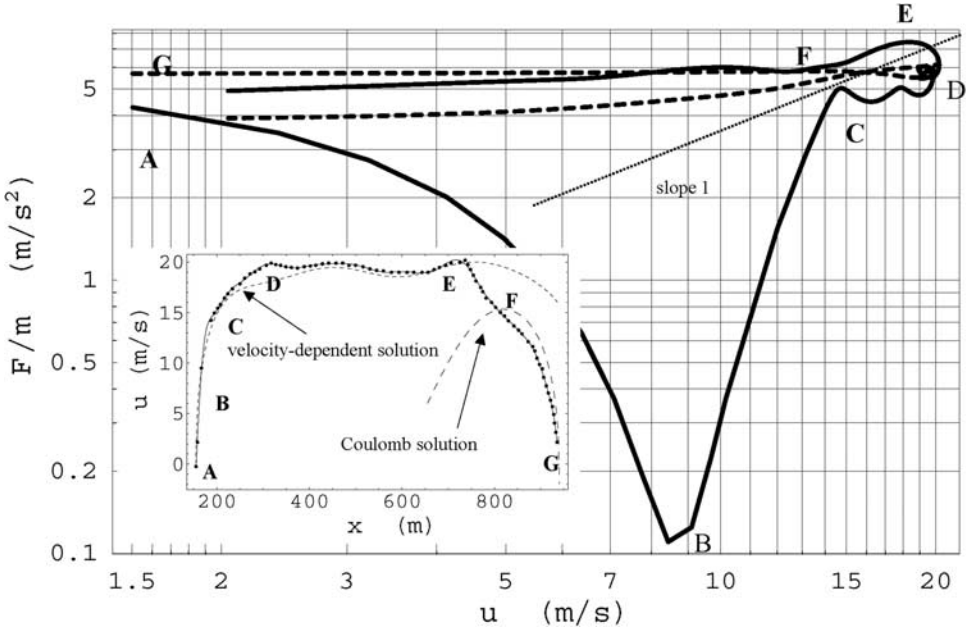

Figure 11. Variation in the frictional force per unit mass F/m with the avalanche velocity u for the avalanche of 7 March 1985 in the Fogas site (solid line); F/m was obtained by applying equation (5) to the measured velocities and path profile, both regularized using N-order Legendre polynomials ($N = 23$ for the velocities, $N = 17$ for the path profile). The dashed curve stands for the variation in the driving force per unit mass $g\sin\theta$. In the inset we have reported the variations in the measured velocities (dots) with downstream distance x. In the inset the solid line represents the Legendre polynomial approximation of velocities, while the dashed line stands for the velocity of a rigid body sliding in a pure Coulombic regime (with $\mu = 0.705$). Letters from A to G refer to various stages of the avalanche run (see text). The starting point is $x_0 = 153$ m; the run-out point is $x_{stop} = 931$ m.

we failed to find a universal scaling; that is, we did not find a typical constant value for exponent n.

[28] A typical example is provided by the Fogas avalanche of 7 March 1985, which at first glance is very similar to the Arabba avalanche examined in section 3.3. As done previously, we have drawn the F/m variations with u (solid line) deduced by applying equation (5) to field data. On the same plot we report the downward component of the driving force $g\sin\theta$ (dashed line). The inset of Figure 11 shows the recorded velocity $u(x)$ (dots) and the Legendre polynomial approximation (solid line). The long-dashed curve stands for the Coulombic solution fitted using the same procedure described in section 3.3. Note that contrary to the Arabba avalanche examined in section 3.3, it was not possible to find a Coulomb solution that mimics the recorded velocities over the whole range $[\xi_0, \xi_{stop}]$ (or, equivalently, $[x_0, x_{stop}]$), and therefore we decided to represent only the part of the solution that comes closer to the observed velocities. As shown in Figure 11, this concerns only a narrow range of distances (branch F–G). The dashed curve represents the "velocity-dependent solution": Assuming a frictional force in the form $F/m = 0.35\,u$ (see below for explanations), we numerically solved equation (5) to find $u(x)$. Note that for this solution the avalanche stops farther than the observed avalanche.

[29] As for the Aulta avalanches and one of the Madergrond avalanches (see Figure 8), there was first a rapid decrease in the frictional force just after the avalanche released: On average, between instants A and B, the frictional force decreased with increasing velocity as ($F/m \propto u^{-2.2 \pm 1.5}$). At instant B the velocity reached by the avalanche was 8 m s^{-1}, a fairly low velocity compared to the velocities reached by avalanches in an inertial regime (compare with Figure 9). Then, between instants B and C the frictional force grew very rapidly with increasing velocity: $F/m \propto u^{5.5}$ until F/m reached its initial level (5 m s^{-2}). At this instant (C) the frictional force followed a plateau phase, but the velocity continued to increase due to the positive difference between the driving force and the frictional force. Between instants D and E the avalanche velocity reached a steady state (velocities in the range 19–20 m s^{-1}) because the path slope was fairly constant, and the frictional force counterbalances the driving action almost exactly. Note that branch D–E represents 415 m in horizontal distance along the path, i.e., approximately half of the distance traveled by the avalanche (see inset of Figure 11). All of this rather long stage in the avalanche's life is represented by a point (point D in Figure 11) in the plot (u, F/m); in fact, a closer look at Figure 11 shows that this stage is not represented by a well-defined point but by a series of intertwining loops occupying a tiny area. At instant E the difference between the driving and the frictional forces dropped below zero, marking the beginning of the decelerating phase. On the whole, on the E–G branch the frictional force varied slowly with velocity as $F/m \propto u^{0.15 \pm 0.05}$, but the dependence on velocity is much more pronounced between instants E and F since we have approximately $F/m \propto u^{1 \pm 0.1}$. We have considered two approximations to describe the behavior between instants C and G.

[30] 1. We assume that the avalanche is in a velocity-dependent regime between instants C and F. Roughly, the corresponding points in Figure 11 form a loop, whose axis is approximately symmetric around the line $F/m = 0.3\ u$. In a first approximation we replace the complex loop behavior with the simple relationship $F/m = 0.3u$. Implementing this expression in equation (5), then solving it to deduce $u(x)$, leads to the dashed curve shown in the inset of Figure 11. This curve mimics the avalanche behavior fairly well from the release (point A) to the point of deceleration (point E) but significantly overestimates both velocities in the decelerating phase and the run-out distance.

[31] 2. In a first approximation the frictional force in the slowly decreasing branch E–G can be considered as constant: $F/m = 6 \pm 1$ m/s^2. As done previously (see section 3.3), we examined how this branch deviated from the solution to equation (5) obtained by assuming a pure Coulombic frictional force. As shown in the inset of Figure 11, the velocities predicted by a Coulombic friction solution (long-dashed curve) are in good agreement with the recorded data only at the very late moments of the decelerating phase (branch F–G in the inset). Surprisingly enough, although the frictional force was fairly constant between instants E and F, it was not possible to reproduce the recorded data by using a Coulombic friction solution. This point will be discussed in section 4.2.

[32] In short, the Fogas avalanche of 7 March 1985 went through three regimes: In the first instants after the release an inertial regime occurred, during which the avalanche accelerated (branch A–B in Figure 11). Next, the avalanche entered a velocity-dependent regime, during which the frictional force revealed a quasi-linear velocity dependence (B–E) on average: $F/m \propto u$. In the run-out phase (E–G) the avalanche decelerated quickly; the frictional force was almost independent of velocity (Coulombic frictional regime).

4. Discussion

[33] The treatment described above shows that (1) the bulk frictional force experienced by an avalanche varies nonlinearly with velocity for most events; (2) the bulk frictional force exhibits hysteretic properties; that is, there is not a single relationship between frictional force and velocity during the acceleration and deceleration phases; and (3) there is also a great diversity in avalanche behavior. Avalanches involving large volumes of new snow (i.e., whose volume exceeds 10,000 m^3) can reach a very high velocity (40 m s^{-1} or more). The considerable acceleration of the avalanche during the release and initial flow phases results from the low value of the frictional force compared to gravity acceleration. In contrast, avalanches involving small volumes of snow exhibit, to a lesser or greater extent, Coulombic frictional properties.

[34] Three regimes have been identified and characterized. After their phenomenological description given in section 3, let us now interpret them from a physical perspective.

4.1. Nature of the Inertial Regime

[35] In the inertial regime the bulk frictional force drops rapidly to zero, which allows the avalanche to accelerate vigorously. Two questions remain unanswered: What are the basic mechanisms involved in the frictional force collapse, and which parameter actually controls the transition from an inertial regime to another regime?

[36] The frictional force collapse is probably an artifact of the inference method used here. This can be seen in Figure 11 for the Fogas avalanche (and later in Figure 13 for the Aulta avalanches): Implementing a force in the form $F/m \propto u$ makes it possible to suitably reproduce the velocities in the release phase, although the inference method provides a variation in F in the form $F/m \propto u^{-2.2}$. In fact, the slope of the release zone is sufficiently large to control the avalanche dynamics whatever the frictional force expression. Since at the release instant $u(\xi_0) = 0$, equation (5) implies that $F/m = g \sin\theta$; a few moments after the release, $u > 0$ and $du/d\xi > 0$ and thus equation (5) implies that F/m must be a decreasing function of u in the first instants after the release.

[37] The very large acceleration in early phases is also observed for powder snow avalanches developing a dilute cloud of snow [*Ancey*, 2003]. In this case, it was shown that the avalanche ceases to accelerate when cloud dilution resulting from the air entrainment is sufficient to significantly reduce the driving buoyancy force [*Beghin et al.*, 1981]. This explanation does not hold here since in a flowing avalanche the air entrainment cannot really lead to a decay in the driving force. A closer look at the variation in the frictional force with bed slope reveals that the frictional force variations for smooth paths are weakly correlated with bed slope, except during the transition and run-out phase: The point of deceleration corresponds approximately to the point of the path profile, from which the local slope starts dropping to zero. At this stage of the investigation, with the data currently available, we have found no clear reason why the avalanche stops accelerating and reaches a fairly well-established steady state.

4.2. Nature and Interest of the Coulomb Regime

[38] The idea that avalanches can behave as Coulombic materials is not new. *Dent* [1986, 1993] put forward the idea that for flowing avalanches, shear should occur in a thin layer at the avalanche base, the remainder of the flow depth being unsheared. *Savage and Hutter* [1989] and *Savage* [1989] also expressed the idea that rapidly sheared natural flows over steep slopes, such as avalanches, should behave as granular flows exhibiting Coulomb friction. Experiments done in the laboratory, either by releasing a given volume of a granular mass or by supplying a constant flow rate of materials, have shown that on steep slopes a granular flow never reached a steady uniform regime and that a Coulomb model can be used to describe the flow properties [*Hungr and Morgenstern*, 1984; *Savage and Hutter*, 1989; *Hutter*, 1996; *Tai et al.*, 2001; *Ancey*, 2002]. This idea is supported here by the results of the back analysis for a number of avalanches at the Khibins and the Arabba sites. From field measurements made using a Doppler radar, *Gubler* [1993] found that the velocity profile inside the Aulta avalanches exhibited a plug zone (constant velocity zone) and a sheared zone at the bottom, clearly revealing that there is shear localization at the bottom. Note that this does not really prove that the Coulomb model is appropriate for describing snow flows since any viscoplastic model (e.g., Bingham's model) also provides a velocity profile involving a sheared and an unsheared zone.

Table 2. Adjustment of the μ Value[a]

Path	μ Value	Comments
	Inertial	
Aulta (a)	0.40	acceptable agreement
Aulta (b)	0.45	acceptable agreement
Madergrond (a)	0.57	possible if x_0 is translated
Madergrond (c)	0.60	possible if x_0 is translated
	Coulombic Frictional	
Arabba (b)	0.712	acceptable agreement
Arabba (c)	0.66	good agreement
Arabba (d)	0.703	velocities overestimated by 140%
Khibins (a)	0.41	good agreement
Khibins (b)	0.42	good agreement
Khibins (c)	0.41	good agreement
Lautaret	0.53	good agreement
	Velocity-Dependent	
Arabba (a)	0.66	good agreement
Slushman	0.53	good agreement
Madergrond (b)	0.645	possible if x_0 is translated
Fogas	0.705	acceptable agreement in the stopping phase

[a]The value was determined by solving equation (5) and taking the observed release point as the starting point, except for the Madergrond avalanches, for which we took $x_0 = x_{start} + 100$ m for the adjustment procedure to operate. Here "good agreement" means that both the run-out distance and the velocities are well described (with a relative deviation between simulated and recorded values of <20% for the velocities); "acceptable agreement" means that the trend is quite good for the velocities, but the relative deviation between computed and measured values locally exceeds 20%.

[39] Assuming that the frictional force is in the Coulombic form $F = \mu\sigma S = \mu mg\cos\theta$, where μ is the friction coefficient, we solved the motion equation (5) with initial condition $u(\xi_0) = 0$. An example of the computation is reported in the inset of Figure 10 for the Arabba avalanche of 21 December 1997. Good agreement was also found for other events that were in a Coulombic frictional regime most of the time. Table 2 summarizes the μ values fitted for each event. For some paths and events, adjusting the μ coefficient requires three digits of precision. The extreme sensitivity of the fitted values comes from the locally large variation in the run-out distance x_{stop} with respect to the μ value. For instance, Figure 12 shows how x_{stop} depends on μ for the Arabba site: clearly, in the range 0.7–0.72, there is a very large variation in the run-out distance (560–690 m). When the μ value has been fitted, we have found that the Coulomb model provides velocities in good agreement with recorded data for all events except one: For the Arabba avalanche of 14 April 1998, it was possible to compute the μ value (μ = 0.703) by matching the computed distance to the recorded value x_{stop} = 678 m (the dashed lines in Figure 12 show how μ is deduced from x_{stop}). However, as shown in inset of Figure 12, the computed velocities overestimated the recorded velocities by 140%. A possible explanation for this discrepancy is that this avalanche involved wet snow; it has been widely observed that wet snow avalanches can travel long distances over gentle slopes in a rather slow motion (in a way comparable to debris flow motion).

[40] Interestingly enough, the Coulomb model can also provide good results for the other two regimes. Clearly, since the frictional force deviates from a constant value, the predicted velocities can compare well with the observed velocities for only certain phases of the avalanche course. In Figure 13 we report the velocity variations for the two avalanches that occurred in the Aulta path. The μ values were computed using the same procedure described in section 3.3 so that the simulated run-out distance equaled the recorded value. It can be seen that the Coulomb model can provide a fairly good estimate of the maximum velocity (underestimating by ~25%), and it describes the velocity decay during the run-out phase quite well. We came to the same conclusion for the avalanches experiencing a velocity-dependent regime. Only the avalanches in the Madergrond path could not be described using a Coulomb model. This is

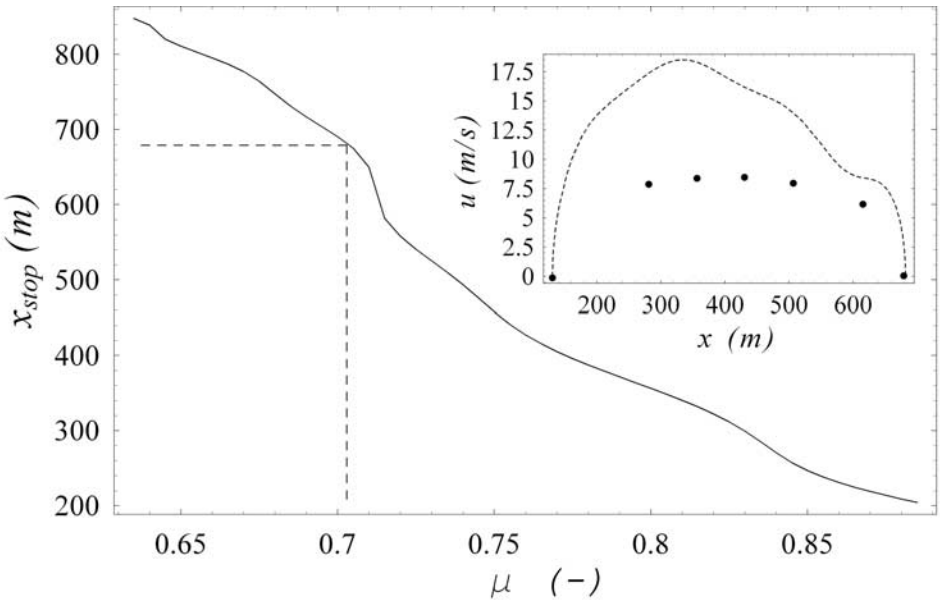

Figure 12. Variation in the run-out distance according to μ for the Arabba site. In the inset we have reported the measured velocities for the Arraba avalanche (d) and the velocities computed with μ = 0.703.

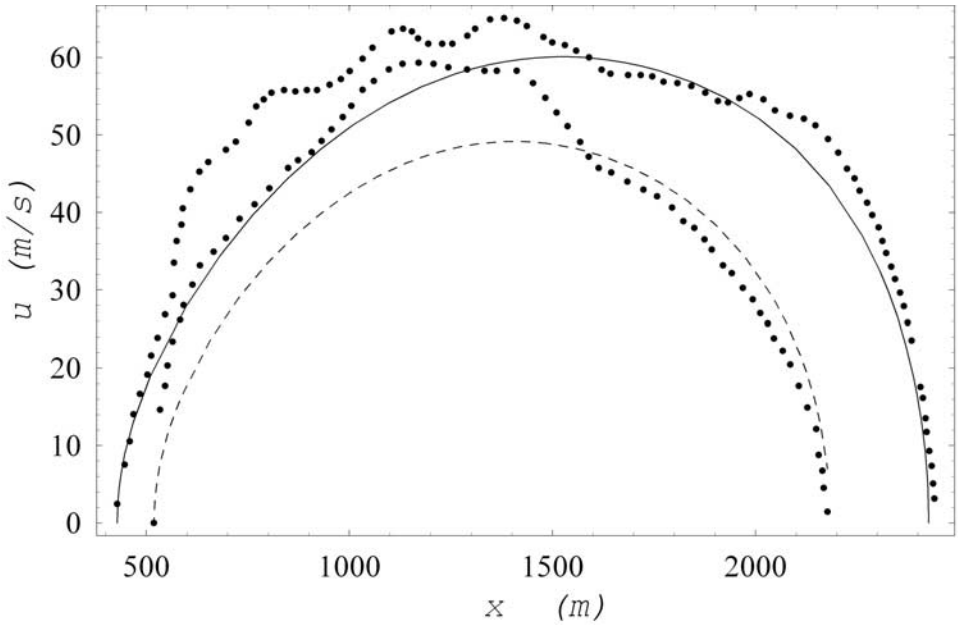

Figure 13. Variation in the avalanche velocity for the two avalanches in the Aulta path. Dots represent the recorded values (same data as in Figure 1). The curves stand for the numerical simulation to equation (5) when the Coulomb model is used: avalanche (b) (solid line), $\mu = 0.45$; avalanche (a) (dashed line), $\mu = 0.40$.

a direct consequence of the path profile shape (see Figure 2). Indeed, the path profile is made up of a long convex steep slope and a fairly flat bottom; the average inclination of the release zone (50–60%) is lower than the slope in the remainder of the path (inclination in the range 50–70%). This implies that if a low friction coefficient value is used, the avalanche travels the entire path down to the flat bottom, whereas if a large value (in excess of 44%) is selected, the avalanche stops immediately after the release. The variation of x_{stop} when varying μ is shown in Figure 14 (dashed curve). It can be seen that at $\mu = 0.44$ the run-out distance suddenly drops from the upper bound of the computation range to x_0.

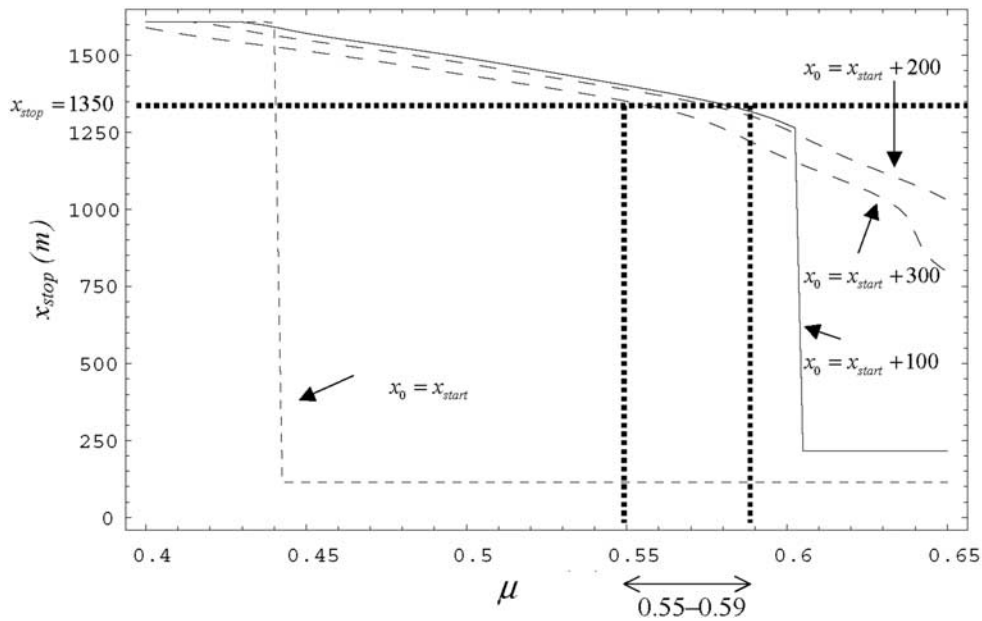

Figure 14. Dependence of the computed run-out distance x_{stop} on coefficient μ (Coulomb model). The dashed line represents the computation using the observed position of the release point as the initial point. The solid line represents the computation assuming $x_0 = x_{\text{start}} + 100$ m. The long-dashed lines represent computations assuming $x_0 = x_{\text{start}} + 200$ m and $x_0 = x_{\text{start}} + 300$ m. Here $x_{\text{start}} = 115$ m and is computed on the Madergrond path.

This inconsistency can be removed by translating the release point downward. For instance, by considering that the initial point is $x_0 = x_{start} + 100$ m (with $x_{start} = 113$ m being the observed starting point), the function $x_{stop}(\mu)$ becomes smoother, making it possible to determine the coefficient μ for the computed run-out distance to match the observed value $x_{stop} = 1350$ m. Further computations were performed by varying the release point. As shown in Figure 14, the function $x_{stop}(\mu)$ depends somewhat on the initial point x_{start}. For instance, by adding a distance in the range 100–300 m to the observed release point, we found that μ lies within the range 0.55–0.59 for the computed run-out distance to match the observed value (see Figure 14).

[41] In short, the Coulomb model is well suited to describing the velocity variation and the run-out distance for avalanches experiencing a Coulombic frictional regime. Provided one is interested mainly in the velocity variation in the decelerating phase (which is the chief concern in avalanche zoning), it can be fitted successfully and used for other avalanches. In addition to its simplicity (one-parameter model), the overriding advantage of the Coulomb model is that its friction coefficient can be adjusted from run-out distance records, and the velocities in the stopping zone can be easily inferred from the fitted value. For a number of practical applications, notably in avalanche zoning when one is interested in determining rare and extreme events from a limited number of observed past events [*Ancey et al.*, 2003], this result is of prime importance.

[42] It is, however, unclear if the Coulomb model really describes the physical behavior of avalanches. A number of physical systems exhibit behavior interpreted as frictional behavior at the macroscopic scale, whereas at the microscopic scale the real behavior is much more complicated. A typical example is given by the motion of a bead rolling down a bumpy line: Some experimental investigations have shown that the bulk frictional force can be expressed in the form $F = \mu mg \cos\theta + Au^2$, where A is a constant. The first term is usually interpreted as a bulk frictional contribution, but a detailed microstructural analysis has demonstrated that this term mainly reflects the collisional dissipation at the bead scale and not a Coulomb frictional process [*Ancey et al.*, 1996b]. For snow avalanches, it is probable that a number of events can be suitably categorized into a Coulomb frictional regime since they behave as a sliding body. For other events such as high-speed dry snow avalanches that occurred in the Aulta path, it is more probable that the Coulomb model offers a conceptual rather than a physical way of describing avalanche behavior. The available data are, however, insufficient to provide clear evidence on this point.

4.3. Comparison With Theoretical Models

[43] Other expressions of the bulk frictional force can be found in the literature. For instance, *Voellmy* [1955] and subsequent authors assumed that the frictional force could be cast in the following form: $F = \mu mg \cos\theta + mgu^2/(\xi h)$ for avalanches down open slopes (i.e., an unconfined path), where (μ, ξ) are two friction coefficients. (For a recent review on the Voellmy model, see *Bartelt et al.* [1999].) *Perla et al.* [1980] proposed a slightly different expression: $F = \mu mg \cos\theta + Du^2$. These models differ from the Coulomb model in that they consider a square velocity contribution, often interpreted as a turbulent term. This additional term has important implications. First, with the Coulomb model, an avalanche flowing down a constant inclination path never reaches a steady state, whereas with a Voellmy or Perla model the avalanche can reach a steady regime. This property has been widely used in the past to fit the coefficients of the Voellmy or Perla model. Second, since Voellmy and Perla's models are two-parameter models, they should provide better descriptions of the velocity variations. The friction coefficient values have been adjusted for each event and are reported in Table 3. We have introduced the parameter α, which is equal to $\xi\ h/g$ in the Voellmy-like model and m/D in the Perla model. Agreement with field data is slightly better compared to the Coulomb model (notably for the Arabba avalanche of 14 April 1998), but on the whole, there is not much difference in the performance of the two models. This is not surprising since a square velocity contribution to the bulk frictional force was not detected in the back analysis presented in section 3.

Table 3. Adjustment of the μ and α Values[a]

Path	μ Value	α Value	Comments
		Inertial	
Aulta (a)	0.30	2,500	good agreement
Aulta (b)	0.22	1,400	good agreement
Madergrond (a)	0.475	1,500	velocities underestimated in the release phase
Madergrond (c)			x_0 must be translated
		Coulombic Frictional	
Arabba (b)	0.60	800	good agreement
Arabba (c)	0.68	700	fairly good agreement
Arabba (d)	0.61	800	fairly good agreement
Khibins (a)	0.34	1,100	good agreement
Khibins (b)	0.37	1,500	velocities underestimated in the stopping phase
Khibins (c)	0.35	1,200	good agreement
Lautaret	0.43	500	acceptable agreement
		Velocity-Dependent	
Arabba (a)	0.63	1,200	good agreement
Slushman	0.44	500	good agreement
Madergrond (b)	0.60	500	good agreement
Fogas	0.70	3000	acceptable agreement in the stopping phase

[a]Here $\alpha = m/D$ for the model of *Perla et al.* [1980] and $\alpha = \xi h/g$ for the *Voellmy* [1955] model.

[44] Comparing the μ values reported in Tables 2 and 3 shows that the values fitted using a Voellmy-like model can be significantly lower than the values obtained using the Coulomb model. For instance, for the Aulta avalanche of 10 February 1984 we found $\mu = 0.45$ for the Coulomb model versus $\mu = 0.22$ for the Voellmy-like model; for the Aulta avalanche of 8 February 1984 the difference is less significant (0.3 versus 0.4). There is apparently no clear reason why the value of μ can differ so much depending on the chosen model since here the turbulent contribution is of much smaller magnitude than the Coulomb term and therefore should only bring a first-order correction. Another surprising point is that the μ and ξ values found here are significantly different from the values given in the Swiss guidelines, which tabulate the frictional coefficient values depending on the path and snow features for extreme avalanches [*Salm et al.*, 1990]. Indeed, taking $h = O(1)$ m, one obtains $\xi = \alpha g/h \approx 10\alpha$. Thus for the events considered here we found that μ lies within the range

0.22–0.7 and ξ is within the range 5,000–30,000 m s^{-2}, while in the Swiss guidelines, μ lies within the range 0.155–0.3 and ξ is within the range 400–1000 m s^{-2}. In a previous benchmark study on the use of Voellmy-like models to compute the features of large avalanches, *Barbolini et al.* [2000] also found differences between the values they fitted and the tabulated values given by the Swiss guidelines. Even though the events in the sample used here cannot be considered as extreme events, the significant difference between the values found here and those provided elsewhere is sufficiently troubling to question the wisdom of using a Voellmy-like model to predetermine the run-out distance of extreme events. Note that for the Perla model the only complete investigation that we have found on the fitting of the m/D parameter is the work by *Lied and Bakkehøi* [1980]: From a sample of 136 paths in the United States and Norway they arrived at the conclusion that the ratio m/D must lie within the range $Y/10$-$10Y$, where Y is the elevation difference between the top and the bottom points of the path. Here the fitted values of m/D belong to the range of possible values provided by Lied and Bakkehøi, but this range is so wide that such an agreement is not surprising.

5. Concluding Remarks

[45] Knowing the velocity variation and the path profile makes it possible to infer the bulk frictional force experienced by an avalanche during its course. Applying this idea to 15 events in North America and Europe, we have found that the bulk behavior of avalanches can be classified into three groups. The bulk frictional force varies substantially during the avalanche course: It comes close to zero in the release phase, while it becomes the prevailing term during the run-out phase. In the inertial regime the avalanche accelerates vigorously and reaches high velocities (in excess of 50 m s^{-1}). In the Coulombic frictional regime the frictional force is fairly constant: The avalanche accelerates and then decelerates, without really reaching a steady state. The velocity-dependent regime lies between these two extreme regimes. The bulk frictional force exhibits complicated dependencies on the velocity (hysteric behavior), and no universal scaling in the expression $F \propto u^n$ has been found. The snow volume involved in the avalanche and the snow type probably influence the flow regime of the avalanche. The limited number of documented avalanches provides only weak trends. It has been found, for instance, that avalanches mobilizing a large snow volume experience an inertial regime in the early moments.

[46] A striking result is that the Coulomb model can be used to describe the velocity variations for avalanches experiencing not only the Coulombic frictional regime but also the two other regimes. In the latter case the model provides a very good description of the velocity decay in the run-out phase but may underestimate the avalanche phase during the release and/or flow phase(s).

[47] This result has very important implications in engineering, notably in avalanche zoning: Knowing the run-out distance makes it possible to deduce the velocity variations of the avalanche, at least in the late phases. This result is crucial when one is interested in deducing the features of rare events from a time series of avalanche run-out distances [e.g., see *Ancey et al.*, 2003]. The important question of the physical meaning of this result remains, however, unanswered due to the level of approximation of this paper. To advance in this direction, it is essential to acquire more data, including the front velocity and flow depth measurements together, if possible, with velocity profiles across the depth inside the avalanches.

[48] **Acknowledgments.** We thank the Institut National des Sciences de L'Univers of the CNRS piloting the PNRN (Programme National sur les Risques Naturels) for its support of this research. We thank K. Hutter and S. Pudasaini for the careful reading of this paper and for bringing helpful comments to improve clarity.

References

Ancey, C. (2001a), Introduction to rheology and applications to geophysics, in *Geomorphological Fluid Mechanics: Selected Topics in Geological and Geomorphological Fluid Mechanics*, edited by N. J. Balmforth and A. Provenzalle, pp. 52–78, Springer-Verlag, New York.

Ancey, C. (2001b), Snow avalanches, in *Geomorphological Fluid Mechanics: Selected Topics in Geological and Geomorphological Fluid Mechanics*, edited by N. J. Balmforth and A. Provenzalle, pp. 319–338, Springer-Verlag, New York.

Ancey, C. (2002), Dry granular flow down an inclined channel: Experimental investigations on the frictional-collisional regime, *Phys. Rev. E*, *65*, pap. 11304.

Ancey, C. (2003), Influence of particle entrainment from bed to the powder-snow avalanche dynamics, *J. For. Snow Landscapes*, in press.

Ancey, C., P. Coussot, and P. Evesque (1996a), Examination of the possibility of a fluid-mechanics treatment for dense granular flows, *Mech. Cohesive Frictional Mater.*, *1*, 385–403.

Ancey, C., P. Evesque, and P. Coussot (1996b), Motion of a single bead on a bead row: Theoretical investigations, *J. Phys. I*, *6*, 725–751.

Ancey, C., M. Meunier, and D. Richard (2003), Inverse problem in avalanche dynamics models, *Water Resour. Res.*, *39*(4), 1099, doi:10.1029/2002WR001749.

Balmforth, N. J., A. S. Burbridge, and R. V. Craster (2000), Viscoplastic models of isothermal lava domes, *J. Fluid Mech.*, *403*, 37–65.

Barbolini, M., U. Gruber, C. J. Keylock, M. Naaim, and F. Savi (2000), Application of statistical and hydraulic-continuum dense-snow avalanche models to five European sites, *Cold Reg. Sci. Technol.*, *31*, 133–149.

Bartelt, P., B. Salm, and U. Gruber (1999), Calculating dense-snow avalanche runout using a Voellmy-fluid model with active/passive longitudinal straining, *J. Glaciol.*, *45*, 242–254.

Beghin, P., E. J. Hopfinger, and R. E. Britter (1981), Gravitational convection from instantaneous sources on inclined boundaries, *J. Fluid Mech.*, *107*, 407–422.

Brugnot, G., and R. Pochat (1981), Numerical simulation study of avalanches, *J. Glaciol.*, *27*, 77–88.

Buser, O., and H. Frutiger (1980), Observed maximum run-out distance of snow avalanches and determination of the friction coefficients μ and ξ, *J. Glaciol.*, *26*, 121–130.

Contreras, S. M., and T. R. H. Davies (2000), Coarse-grained debris-flows: Hysteresis and time-dependent rheology, *J. Hydraul. Eng.*, *126*, 938–941.

Coussot, P. (1997), *Mudflow Rheology and Dynamics*, A. A. Balkema, Brookfield, Vt.

Denlinger, R. P., and R. M. Iverson (2001), Flow of variably fluidized granular masses across three-dimensional terrain: 2. Numerical predictions and experimental tests, *J. Geophys. Res.*, *106*, 553–566.

Dent, J. D. (1986), Flow properties of granular materials with large overburden loads, *Acta Mech.*, *64*, 111–122.

Dent, J. D. (1993), The dynamic friction characteristics of a rapidly sheared granular material applied to the motion of snow avalanches, *Ann. Glaciol.*, *18*, 215–220.

Dent, J. D., and T. E. Lang (1980), Modelling of snow flow, *J. Glaciol.*, *26*, 131–140.

Dent, J. D., and T. E. Lang (1982), Experiments on the mechanics of flowing snow, *Cold Reg. Sci. Technol.*, *5*, 243–248.

de Quervain, R., (Ed.) (1981), *Avalanche Atlas*, Unesco, Paris.

Eglit, E. M. (1983), Some mathematical models of snow avalanches: Advances, in *Mechanics and the Flow of Granular Materials*, edited by M. Shahinpoor, pp. 577–588, Trans Tech, Clausthal-Zellerfeld, Germany.

Gubler, H. (1993), Dense-flow avalanches: A discussion of experimental results and basic processes, in *International Workshop on Rapid Gravitational Mass Movements*, edited by L. Buisson and G. Brugnot, pp. 127–126, Cemagref, Grenoble, France.

Gubler, H., M. Hiller, G. Klausegger, and U. Suter (1986), *Messungen an Fliesslawinen*, *Rep. 41*, Eidg. Inst. für Schnee- und Lawinenforsch., Davos, Sitzerland.

Hungr, O., and R. R. Morgenstern (1984), Experiments on the flow behaviour of granular materials at high velocity in an open channel, *Géotechnique*, *34*, 405–413.

Hunt, B. (1994), Newtonian fluid mechanics treatment of debris flows and avalanches, *J. Hydrol. Eng.*, *120*, 1350–1363.

Hutter, K. (1996), Avalanche dynamics, in *Hydrology of Disasters*, edited by V. P. Singh, pp. 317–392, Kluwer Acad., Norwell, Mass.

Hutter, K., and R. Greve (1993), Two-dimensional similarity solutions for finite-mass granular avalanches with Coulomb and viscous-type frictional resistance, *J. Glaciol.*, *39*, 357–372.

Hutter, K., T. Koch, C. Plüss, and S. B. Savage (1995), The dynamics of avalanches of granular materials from initiation to runout, *Acta Mech.*, *109*, 127–165.

Iverson, R. M. (1997), The physics of debris flows, *Rev. Geophys.*, *35*, 245–296.

Iverson, R. M., and R. P. Denlinger (2001), Flow of variably fluidized granular masses across three-dimensional terrain: 1. Coulomb mixture theory, *J. Geophys. Res.*, *106*, 537–552.

Kotlyakov, V. M., B. N. Rzhevkiy, and V. A. Samoylov (1977), The dynamics of avalanching in the Khibins, *J. Glaciol.*, *19*, 431–439.

LaChapelle, R. E., and T. E. Lang (1980), A comparison of observed and calculated avalanche velocities, *J. Glaciol.*, *25*, 309–314.

Lied, K., and S. Bakkehøi (1980), Empirical calculations of snow avalanche run-out distances based on topographic parameters, *J. Glaciol.*, *26*, 165–177.

Maeno, O. (1993), Rheological characteristics of snow flows, in *International Workshop on Gravitational Mass Movements*, edited by L. Buisson, pp. 209–220, Cemagref, Grenoble, France.

Major, J. J., and T. C. Pierson (1992), Debris flow rheology: Experimental analysis of fine-grained slurries, *Water Resour. Res.*, *28*, 841–857.

Marco, O. (1986), Dynamique des avalanches de neige dense—Interprétation des résultats, internal report, Cemagref, Grenoble, France.

McClung, D. M., and P. A. Schaerer (1993), *The Avalanche Handbook*, Mountaineers, Seattle, Wash.

Norem, H. F., F. Irgens, and B. Schieldrop (1986), A continuum model for calculating snow avalanche velocities, in *Symposium on Avalanche Formation, Movement and Effects*, *Publ. 186*, Int. Assoc. of Hydrol. Sci., Wallingford, Oxfordshire, U.K.

Parker, G., Y. Fukushima, and H. M. Pantin (1986), Self-accelerating turbidity currents, *J. Fluid Mech.*, *171*, 145–181.

Perla, R., T. T. Cheng, and D. M. McClung (1980), A two-parameter model of snow-avalanche motion, *J. Glaciol.*, *26*, 197–202.

Salm, B., A. Burkard, and H. Gubler (1990), Berechnung von Fliesslawinen, eine Anleitung für Praktiker mit Beispielen, *Internal Rep. 47*, Eigd. Inst. für Schnee- und Lawinenforsch., Davos, Switzerland.

Savage, S. B. (1989), Flow of granular materials, in *Theoretical and Applied Mechanics*, edited by P. Germain, J.-M. Piau, and D. Caillerie, pp. 241–266, Elsevier Sci., New York.

Savage, S. B., and K. Hutter (1989), The motion of a finite mass of granular material down a rough incline, *J. Fluid Mech.*, *199*, 177–215.

Schaerer, P. A. (1974), Friction coefficients and speed of flowing avalanches, in *Symposium Mécanique de la Neige*, pp. 425–432, Int. Assoc. of Hydrol. Sci., Wallingford, Oxfordshire, U.K.

Sovilla, B., F. Sommavilla, and A. Tomaselli (2001), Measurements of mass balance in dense avalanche events, *Ann. Glaciol.*, *32*, 230–236.

Spera, F. J., A. Borgia, J. Strimple, and M. Feigensen (1988), Rheology of melts and magmatic suspensions: 1. Design and calibration of concentric cylinder viscometer with application to rhyolitic magma, *J. Geophys. Res.*, *93*, 10,273–10,294.

Tai, Y.-C., K. Hutter, and J. M. N. T. Gray (2001), Dense granular avalanches: Mathematical description and experimental validation, in *Geomorphological Fluid Mechanics: Selected Topics in Geological and Geomorphological Fluid Mechanics*, edited by N. J. Balmforth and A. Provenzalle, pp. 339–366, Springer-Verlag, New York.

Voellmy, A. (1955), Über die Zerstörungskraft von Lawinen, *Schweiz. Bauztg.*, *73*, 159–162, 212–217, 246–249, 280–285.

C. Ancey, Environmental Hydraulics Laboratory, Swiss Federal Institute of Technology, CH-1015 Lausanne, Switzerland. (christophe.ancey@epfl.ch)

M. Meunier, Research Unit Torrential Erosion, Snow and Avalanches, Cemagref, Domaine Universitaire BP 76, F-38402 Saint-Martin-d'Hères, France. (maurice.meunier@cemagref.fr)